Orbit Determination of Space Debris: Correlation of Optical Observations

J.M. Maruskin
Department of Mathematics
The San Jose State University
D.J. Scheeres
Department of Aerospace Engineering Sciences
The University of Colorado at Boulder
K.T. Alfriend
Texas A&M University

Abstract

When a piece of space debris is observed by optical telescopes, angular and angular-rate information can be preciesely estimated from the track using basic kinematics. However range and range-rate information is to a large extent undetermined, other than by a few weak physical constraints. The standard approach in performing an orbit determination between two separate tracks of data is the least squares approach. This approach, however, presupposes a nominal estimation of the true orbit that is later corrected by the least squares algorithm. Since such an initial estimate is not known *a priori* for a single pass, this approach is ill-suited to deal with the increase in uncorrelated tracks expected as new telescopes come online within the next few years. The approach we describe here takes a more global perspective. After computing the admissible region, the set of all points possible belonging to a given track, for each of the two tracks, we then dynamically evolve or regress these two-dimensional regions into a common coordinate system and finally search for possible intersections. By utilizing this process, large reductions can be made to the uncertainty in the topocentric range, range-rate space. Once candidate solutions are found a standard least squares approximation can refine the initial orbit produced by our method. This paper discusses some of the complications and advantages associated with performing these intersections.

1 Introduction

A problem of recent interest to space-faring nations is the tracking, orbit determination, and cataloging of all pieces of artificial space debris particles in low, medium, and high Earth orbits, a population of more than 300,000 particles with diamter larger than 1 cm. The United States Air Force Space Command has installed a network of 25 radar and optical sensors for this task, which make about 80,000 observations daily. For more background on observation of space debris, see Rossi [1, 2].

Using optical measurements for particles in medium to high Earth orbit, the angles and angular rates of the passing particles, as seen from an Earth-based telescope, can be measured to high precision, however the range and range-rates are largely undetermined. The set of angles and angular rates of such a measurement is called an *attributable vector*. Recent work has been done in outlining a precise mathematical description of the *admissible region* of the range, range-rate plane given an attributable vector observed by radar or optical measurements, Tommei *et al.* [3]. The admissible region is a two-dimensional surface that lives in the six-dimensional phase space surrounding the Earth. This surface consists of all points in phase space where the true particle can possibly be found. For this reason we will sometimes refer to it as the uncertainty surface. This uncertainty surface is then discretized by a number of points called *Virtual Debris particles*, or VD particles. Each VD particle is an approximation to a possible orbit for the observed particle of space debris. Viewed as a whole, the set of VD particles forms a *virtual debris field*, or VD field, which approximates the macroscopic uncertainty distribution associated with a given attributable vector. For optical measurements, the admissible region on the range/range-rate plane is restricted only by the fact

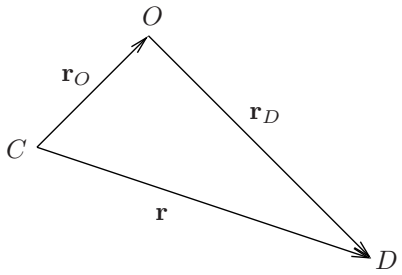

Figure 1: The space debris particle D is observed by the point O on the surface of Earth. The center of Earth is C.

that the debris particle should be gravitationally bound to the Earth (negative geocentric energy), that it lie within some region (2 and 20 Earth radii) of the observer, and that it not impact the Earth [3, 4].

Given this 2-dimensional region, we can assign each value of range and range-rate to a unique set of orbital elements. In our work we use Delaunay elements for reasons outlined in [4]. Thus, each observation corresponds to a 2-dimensional manifold mapped into a 6-dimensional space, with a dynamical evolution that is simply described using standard orbit theory. Our approach uses these ideas, and some nice properties of the Delaunay elements, to develop a conceptual algorithm where the intersection of these 2-D surfaces are computed. If the two observations belong to the same object, they should intersect at a unique point. If they do not correspond to the same object, their intersection should yield the null set.

In this paper we summarize the results from [4] related to our approach and discuss some challenges that we hope to address in the future.

2 Admissible Region

In this section we review the *admissible region* for a space debris particle observed by a ground based optical sensor, as presented in Tommei *et al.* [3], and offer an additional physical constraint that will further limit the size of this region in the range range-rate plane.

2.1 Attributable Vectors

Let $\mathbf{r}$ be the geocentric position of a space debris particle and $\mathbf{r}_O$ the geocentric position of the optical observer. Let the position of the debris particle with respect to the observer be denoted $\mathbf{r}_D = \rho\hat{R}$, where $\hat{R}$ is a unit vector pointing from the observer to the particle. This gives us

$$\mathbf{r} = \mathbf{r}_O + \mathbf{r}_D,$$

as shown in Fig. 1. Let

$$(\rho, \alpha, \delta) \in \mathbb{R}^+ \times [-\pi, \pi) \times (-\pi/2, \pi/2)$$

be the spherical polar coordinates defining $\mathbf{r}_D$. Typically one can choose the J2000 coordinate systems so that α is the right ascension and δ is the declination.

Definition 1 *An optical attributable vector is a vector*

$$A = (\alpha, \delta, \dot{\alpha}, \dot{\delta}) \in [-\pi, \pi) \times (-\pi/2, \pi/2) \times \mathbb{R}^2$$

observed at time t.

The optical attributable vector is precisely the set of coordinates that can be measured from the observer's frame *on the Earth's surface* at time t. Note that unless the debris particle is seen directly overhead, what we call a zenith measurement, this will translate into uncertainty in the polar angles of the *geocentric* frame. Since the coordinate

transformation to the inertial geocentric frame depends on the position of the Earth, additional information must be stored along with the attributable vector. The full set of data that should be tabulated with each observation is

$$x = (A, t, L) \in \mathbb{R}^5 \times \mathbb{N},$$

where $A = (\alpha, \delta, \dot{\alpha}, \dot{\delta})$ is the attributable vector, t is the time of observation, and L is observatory. A function can then be defined as follows

$$\psi : (t, L) \to (h, \Theta, \Phi),$$

where h is the altitude of the observatory (which we ignore in the current discussion), and (Θ, Φ) is the inertial angular location of observatory L at time t. The observation data x and inertial orientation function of the observatory ψ can then be unraveled to form the actual useable information for the coordinate transformations

$$\mathfrak{X} = (A, t, h, \Theta, \Phi) \in \mathbb{R}^8.$$

For simplicity we will take $h = 0$ for the examples worked out in this paper.

2.2 Measuring Attributable Vectors

One of the technical difficulties in Space Situational Awareness (SSA) is the inability to accurately estimate the full dynamical state of an object based on a single track of data. The usual standard for optical only orbit determination is Gauss' method, which requires three measurements of two angles that are sufficiently spread over time and allows one to make a complete orbit determination. In the space debris tracking problem, however, optical search and survey telescopes will observe objects for only very short durations (minutes at most) (Seitzer *et al.* [5]). This track of data contains information on the angular location of the satellite, but in general does not have sufficient information to allow for an accurate orbit determination of the object (e.g. using Gauss' method). For meaningful orbit characterization, the object must be observed again during a later pass. The problem, of course, is to discern which uncorrelated tracks are the same object.

Our approach to this problem is two-fold. First is to extract the maximum amount of usable information from a single track of a space object and to also bound the possible domain of the unmeasured state components. Second is to use this information to correlate one observation track with another from a previous observation in order to detect whether the two objects are the same. In the following we will focus specifically on optical observations of space debris, although the theory and analysis can also apply to radar observations of space debris.

The challenge is to extract the maximum amount of usable information from a single track and also derive meaningful constraints on the remaining uncertainty aspects of the state. Instead of determining an overall covariance matrix for the object's state, based on a single track, that contains all 6 dimensions, our approach is to use the track observations to isolate those components of the object's state that can be constrained. For an optical track consisting of several angular observations over a time span of minutes these are the angular location and angular rate of the object at a specific epoch, generally chosen to lie within the track. The idea is to use the multiple angular measurements to develop an improved estimate of the angular location of the object and the angular rate of the object, and then use these measurements to constrain the unmeasured states of the object. This approach was recently proposed in [3] by Tommei et. al and is further extended in our research. This approach was also discussed in the context of computing attributable vectors for asteroids from short arcs in Milani *et al.* and Milani & Knežević [6].

During an observation period, when a space object passes through the field of view of an optical telescope, the optical telescope can take several measurements of that object, equivalent to a series of angles at specific times, the total time span being a number of minutes. We assume that these angles can be identified with each other to produce a single track of observable data for the space object. There is obviously more information in this pass of data than just a single fix of the angular location of the space object relative to the observer, however there is not enough information to provide an accurate orbit. To capture this additional information, we can estimate the space object's angular location, angular rate and angular acceleration at a fixed epoch, chosen within the tracking pass. The additional information content goes into reducing the uncertainty of the angle, angle-rate and angle-acceleration measurement at epoch. This approach recognizes that there is little information in one track related to the object range and range-rate, and concentrates on fixing the angles, angle-rates, and angle-accelerations to a higher level of precision. A similar approach has been taken to estimate the information content of a single pass of Doppler

data for an interplanetary spacecraft (Hamilton & Melbourne [7]). Estimates, based on published tracking data characteristics for the MODEST space surveillance telescope which tracks GEO objects (Seitzer [5]) yields angular location and angular rate measurement errors on the order of $1.5 \times 10^{-4\circ}$ and $1 \times 10^{-6\circ}$/s, respectively.

This approach combines the information from a track of observations spread out in time and transforms it into a precise estimate of the partial state of the object at a specific epoch. This is a more convenient form in which to transform the information from the track and makes it easier to discuss constraints on the unmeasured components of the space object's state. For an optical observation these unmeasured components are the object's range and range-rate at the epoch t_o and define the attributable vector A.

2.3 The Admissible Region

Given an optical attributable vector A, its corresponding *admissible region* is the set of points on the $(\rho, \dot{\rho})$ plane that have not been ruled out by physical considerations. We impose the following physical constraints on the possible positions of the particle in the topocentric range/range-rate $(\rho, \dot{\rho})$ plane:

- $\mathcal{C}_1 = \{(\rho, \dot{\rho}) : E < 0\}$
- $\mathcal{C}_2 = \{(\rho, \dot{\rho}) : 2 \text{ R}_\oplus < \rho < 20 \text{ R}_\oplus\}$
- $\mathcal{C}_3 = \{(\rho, \dot{\rho}) : 1.03 \text{ R}_\oplus < r_p\}$
- $\mathcal{C}_4 = \{(\rho, \dot{\rho}) : r_a < 25 \text{ R}_\oplus\}$,

where E is the orbital energy, r_p and r_a are the periapsis and apoapsis (geocentric) radii of the orbit, respectively; and where distance is measured in units of Earth-radii. These constraints are introduced in Tommei *et al.* [3], though the majority of their work concentrates on analytical aspects of the first two constraints, $\mathcal{C}_1$ and $\mathcal{C}_2$. The latter conditions $\mathcal{C}_3$ and $\mathcal{C}_4$ constrain the periapsis and apoapsis (geocentric) radii of the orbit to always lie within some range. These latter constraints place a restriction on the possible eccentricities of the orbit, which rule out impact orbits and orbits with an extremely high apoapsis. A periapsis of 1.03 $\text{R}_\oplus$ corresponds to a periapsis radius at about 200 km above the surface of the Earth. The admissible region is then defined as a subset of the topocentric range/range-rate plane by the condition:

$$\mathcal{C} = \bigcap_{i=1}^{4} \mathcal{C}_i. \tag{1}$$

Given an optical attributable vector A, each point in the $(\rho, \dot{\rho})$ plane corresponds to a unique physical orbit in space that can be determined by a set of geometric and orbital element relations. We start by computing the vectors

$$\hat{R} = \langle \cos\alpha \cos\delta, \sin\alpha \cos\delta, \sin\delta \rangle, \qquad \hat{R}_\alpha := \frac{\partial \hat{R}}{\partial \alpha}, \qquad \hat{R}_\delta := \frac{\partial \hat{R}}{\partial \delta}.$$

The geocentric position and velocity of the a particle at $(\rho, \dot{\rho})$ on the range and range-rate plane with attributable vector A is therefore given by

$$\mathbf{r} = \mathbf{r}_O + \rho \hat{R} \tag{2}$$

$$\dot{\mathbf{r}} = \dot{\mathbf{r}}_O + \dot{\rho}\hat{R} + \rho\dot{\alpha}\hat{R}_\alpha + \rho\dot{\delta}\hat{R}_\delta. \tag{3}$$

Given the position in inertial space, the orbital elements of that orbit are then given by standard relations. In order to compute the admissible region, we begin by discretizing the strip given by $\mathcal{C}_2$ for a wide range of range-rates (e.g. $-10 \text{ R}_\oplus \leq \dot{\rho} \leq 10 \text{ R}_\oplus$). For each point in the discretization, we compute the physical orbit corresponding to that point and the energy, periapsis radius, and apoapsis radius of that orbit. If the current point in the $(\rho, \dot{\rho})$ plane satisfies the constraints $\mathcal{C}_1$, $\mathcal{C}_3$, and $\mathcal{C}_4$, it is then stored in a separate list that generates the virtual debris field. This second list is a discretization of the admissible region.

Fig. 2 shows the admissible region for a given optical observation. In this example, the optical observer's position in standard coordinates is polar angle $\Theta = \pi/3$ rads (measured as the polar angle from the north pole) and azimuthal angle $\Phi = 0$ (measured from inertial x-axis), and the observer makes the following zenith observation

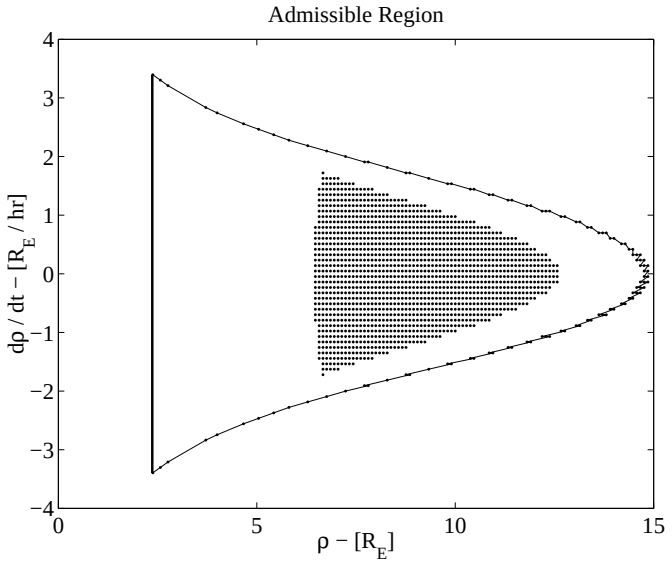

Figure 2: Admissible Region for attributable vector $A = (0 \text{ rads}, \pi/6 \text{ rads}, 0.1 \text{ rads/hr}, 0.03 \text{ rads/hr})$, zenith measurement

$A = (0 \text{ rads}, \pi/6 \text{ rads}, 0.1 \text{ rads/hr}, 0.03 \text{ rads/hr})$. The outlined region in Fig. 2 is what the admissible region would look like if one choose only to incorporate the constraints $\mathcal{C}_1 \cap \mathcal{C}_2$ (as primarily discussed in Tommei *et al.* [3]). The inside dotted region is the (discretized) admissible region when all four constraints are considered, i.e. $\mathcal{C} = \mathcal{C}_1 \cap \mathcal{C}_2 \cap \mathcal{C}_3 \cap \mathcal{C}_4$. As one can see, these additional constraints significantly reduce the area of the admissible region that one must consider in making the orbit determination.

2.4 Delaunay Variables

In this subsection, we briefly define the set of canonical Delaunay variables that we use for mapping the admissible region into orbit element space. The reasons for using these variables are discussed in more depth in [4].

One can transfer the uncertainty surface (admissible region) into geocentric cartesian coordinates and then let each point of this surface evolve as a Keplerian orbit. If one does so, one sees that the surface spreads out fairly quickly. As an alternative, we will transfer the surface into Delaunay variables. This is done in several steps. We first transfer the topocentric spherical observation coordinates into geocentric cartesian coordinates using (2)-(3):

$$T_1 : \langle \rho, \dot{\rho}, \mathfrak{X} \rangle \rightarrow \langle x, y, z, \dot{x}, \dot{y}, \dot{z} \rangle.$$

This transformation depends on the full set of recorded data $\mathfrak{X} = (A, t, h, \Theta, \Phi)$, as it depends on the location of the observer at that time. As usual, $A = \langle \alpha, \delta, \dot{\alpha}, \dot{\delta} \rangle$ is the admissible vector associated with a given track of data. Next, we transfer the cartesian coordinates into a set of orbital elements, using standard relations.

$$T_2 : \langle x, y, z, \dot{x}, \dot{y}, \dot{z} \rangle \rightarrow \langle a, e, i, \omega, \Omega, M \rangle,$$

where a is the semi-major axis, e is the eccentricity, i is the inclination, ω is the argument of periapsis, Ω is the longitude of the ascending node, and M is the mean anomaly. Lastly we transfer the orbital elements into Delaunay variables,

$$T_3 : \langle a, e, i, \omega, \Omega, M \rangle \rightarrow \langle L, l, G, g, H, h \rangle,$$

where the Delaunay variables are defined as in Ferraz-Mello [8]:

$$\begin{aligned} l &= M, & L &= \sqrt{\mu a}, \\ g &= \omega, & G &= L\sqrt{1-e^2}, \\ h &= \Omega, & H &= G\cos i, \end{aligned} \tag{4}$$

so that the total transformation from the observation space to Delaunay space at the initial time t_0 is given by the composition:

$$T(t_0; t_0) = T_3 \circ T_2 \circ T_1. \tag{5}$$

For the case of zero-eccentricity or zero-inclination orbits, the Delaunay variables become singular, and one could instead choose Poincaré nonsingular canonical variables. In this work we will restrict our attention to cases where singularities are not present and one can use Delaunay variables.

3 Intersection Theory Analysis (ITA)

In this section we describe how the Delaunay space can be used in performing an orbit determination between two previously uncorrelated tracks (UCT's).

3.1 Mapping the Admissible Region to Delaunay Space

Let $\mathcal{D} \cong \mathbb{R}^6$ be the six-dimensional Delaunay space and $\mathcal{C}(\mathfrak{X})$ the corresponding admissible region in the topocentric range/range-rate plane for a fixed attributable vector and spatiotemporal observation location, as defined in (1). For a fixed epoch time τ, we define the map $F_{\mathfrak{X}}^{\tau} : \mathcal{C} \to \mathcal{D}$ as the map from the Admissible Region for a fixed $\mathfrak{X}$ to the Delaunay elements, where t is the time of the observation (one of the components of $\mathfrak{X}$), so that:

$$F_{\mathfrak{X}}^{\tau} : \langle \rho, \dot{\rho} \rangle \to \langle L, l, G, g, H, h \rangle.$$

Thus $F_{\mathfrak{X}}^{\tau}(\mathcal{C}) \subset \mathcal{D}$ is a two-dimensional submanifold of Delaunay space $\mathcal{D} \cong \mathbb{R}^6$. We further define the three *Delaunay projective spaces* $\mathcal{D}_L \cong \mathcal{D}_G \cong \mathcal{D}_H \cong \mathbb{R}^2$, so that the Delaunay space $\mathcal{D}$ has the direct sum decomposition $\mathcal{D} = \mathcal{D}_L \oplus \mathcal{D}_G \oplus \mathcal{D}_H$. These three projective spaces are the projections of Delaunay space onto the three symplectic Delaunay planes. The map $F_{\mathfrak{X}}^{\tau}$ can be thought of in either of two ways, as a one-to-one mapping from the two-dimensional admissible region $\mathcal{C}$ to the six-dimensional Delaunay space $\mathcal{D}$ or as a one-to-three mapping from the two-dimensional admissible region $\mathcal{C}$ to the three two-dimensional Delaunay projective spaces $\mathcal{D}_L$, $\mathcal{D}_G$, and $\mathcal{D}_H$. While at first glance, such a distinction seems pedantic, it is actually an important one, as intersections are inherently easier to both visualize and carry out in two-dimensional spaces than they are in six-dimensional spaces.

3.2 Necessary Conditions for Correlation between Two UCT's

Given two extended attributable vectors $\mathfrak{X}_1$ and $\mathfrak{X}_2$, one determines the corresponding admissible regions $\mathcal{C}_1$ and $\mathcal{C}_2$, respectively. These admissible regions cannot be compared directly, as they are subsets of two different sets of topocentric spherical coordinates, affixed to the Earth at different locations and different times. We now push the admissible regions forward into Delaunay space, and dynamically evolve or regress both uncertainty distributions in time to a common epoch τ, so that $F_{\mathfrak{X}_1}^{\tau}(\mathcal{C}_1)$ and $F_{\mathfrak{X}_2}^{\tau}(\mathcal{C}_2)$ are both two-dimensional submanifolds of six-dimensional Delaunay space $\mathcal{D}$, dynamically mapped to a common epoch time.

If $\mathfrak{X}_1$ and $\mathfrak{X}_2$ correspond to the same object, then $F_{\mathfrak{X}_1}^{\tau}(\mathcal{C}_1)$ and $F_{\mathfrak{X}_2}^{\tau}(\mathcal{C}_2)$ must necessarily intersect. Since $\mathfrak{X}_1$ and $\mathfrak{X}_2$ each contain four pieces of information (two angles and two angle rates), the system is overdetermined. Unless there is some redundancy in the information, if both tracks correspond to the same physical object, it is likely that the uncertainty manifolds $F_{\mathfrak{X}_1}^{\tau}(\mathcal{C}_1)$ and $F_{\mathfrak{X}_2}^{\tau}(\mathcal{C}_2)$ will intersect at a single point $\mathbf{\Delta}^*$.

On the other hand, suppose that it is still unknown whether both attributable vectors correspond to the same physical object, but the surfaces $F_{\mathfrak{X}_1}^{\tau}(\mathcal{C}_1)$ and $F_{\mathfrak{X}_2}^{\tau}(\mathcal{C}_2)$ are found to intersect at a single point. Then we can then conclude with a high confidence that both attributable vectors correspond to the same object. The reason is that $F_{\mathfrak{X}_1}^{\tau}(\mathcal{C}_1)$ and $F_{\mathfrak{X}_2}^{\tau}(\mathcal{C}_2)$ are both two-dimensional manifolds embedded into the same six-dimensional Delaunay space

$\mathcal{D}$. The probability that they, *by accident*, happen to touch tangentially at a single intersection point $\mathbf{\Delta}^*$ is extremely low, unless they are correlated and the orbit for both objects is given by that common intersection point $\mathbf{\Delta}^*$. A preliminary orbit determination is then given by the intersection point $\mathbf{\Delta}^*$ and the two tracks may be considered to be correlated. One then places this preliminary orbit determination into a separate holding catalog and awaits confirmation by a third consistent track of data, at which time the orbit is added to the standard catalog.

3.3 Orbit Determination: Finding the Kepler Orbit with Two Observations

In the following we take one example from [4] and present it as an example of how this approach to orbit correlation works. In this particular example we will study the case of two near-zenith observations. If the observation is not made when the space debris particle is directly overhead, the projection of the uncertainty region on the (H, h) plane will not be one-dimensional. The first attributable vector is given by $A = (0 \text{ rads}, \pi/6 \text{ rads}, 0.1 \text{ rads/hr}, 0.03 \text{ rads/hr})$, made at time $t = 0$ hrs from a point on the Earth's surface $\Theta = \pi/3 + 0.1$ rads, $\Phi = 0.1$ rads. Assuming particle #1000 is the true space debris particle, a possible second observation (nonzenith) might be given by the attributable vector $A_{70} = (1.1516 \text{ rads}, 0.4790 \text{ rads}, 0.2262 \text{ rads/hr}, -0.0809 \text{ rads/hr})$, made at time $t = 70$ from a point on the Earth's surface $\Theta = 1.2516$ rads, $\Phi = 1.1918$ rads. The intersections of the admissible regions, as projected onto the Delaunay planes, is shown in Fig. 3. Because the true debris particle did not fly directly over zenith on either

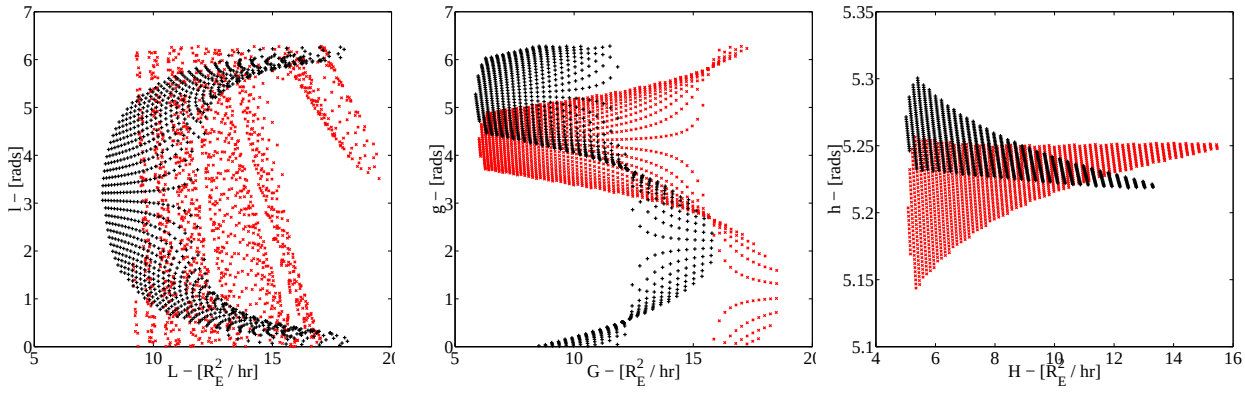

Figure 3: $T(70;0)\{\mathcal{A}\}$ (red) and $T(70;70)\{\mathcal{A}_{70}\}$ (black) projected onto the Delaunay planes, nonzenith observations

of the measurements, the admissible regions now have two-dimensional projections on the (H, h) plane. Since we are considering the Kepler case, the original uncertainty distribution's projections on the (G, g) and (H, h) plane are static. Our goal now is to systematically reduce the uncertainty region, by considering each Delaunay plane in sequence, as much as possible until it is reduced to either a single point (complete orbit determination) or a one-dimensional line.

By examination of the concurrent Delaunay plots of the uncertainty region projections (Fig. 3), we choose to begin the orbit determination process by cutting off the non-overlap sections of the surface in the (H, h) plane. The Delaunay projections of the remaining piece of surface is shown in Fig. 4. We see in Fig. 4 that there is again an overlap and non-overlap region in the (G, g) plane. Removing the non-overlap region further reduces the admissible region, as shown in Fig. 5. Interestingly, the (H, h) projection can be again used to cut out more of the uncertainty surface, resulting in a third reduction, as shown in Fig. 6. We now turn to the projection of the thrice reduced uncertainty region on the (L, l) plane. The first three reductions have eliminated all but three overlap regions on the (L, l) plane. We consider each in term. The systematic projection of each overlap region onto each of the three Delaunay planes is shown in Fig. 7. We see that the far right overlap region on the (L, l) plane (the overlap that is almost confined to a single point) does not overlap on the (G, g) plane. This overlap region thus cannot correspond to the actual debris particle and is now ruled out. The middle overlap region on the (L, l) plane does not overlap on the (G, g) or (H, h) plane, so it is ruled out. Finally, the leftmost overlap region has a small intersection on both the (G, g) and (H, h) plane. The orbit is thus determined to within a small uncertainty about a single point in Delaunay

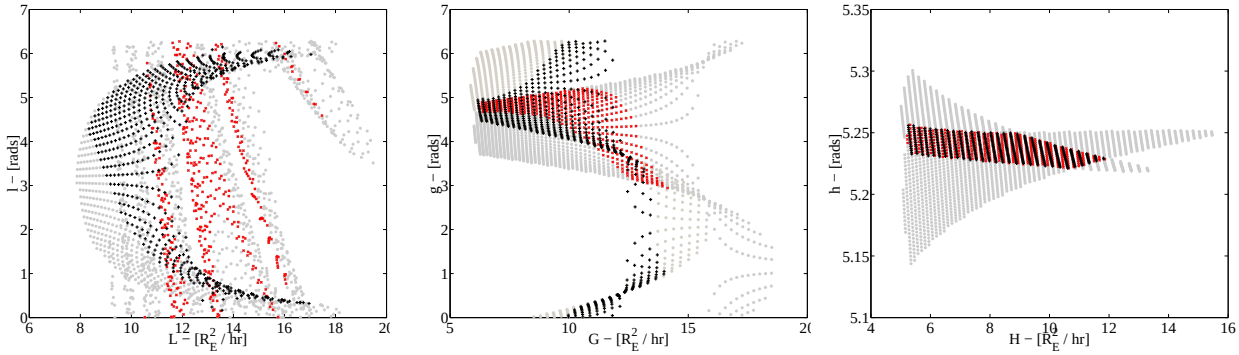

Figure 4: $T(70;0)\{\mathcal{A}^r\}$ (red) and $T(70;70)\{\mathcal{A}^r_{70}\}$ (black) projected onto the Delaunay planes, nonzenith observations

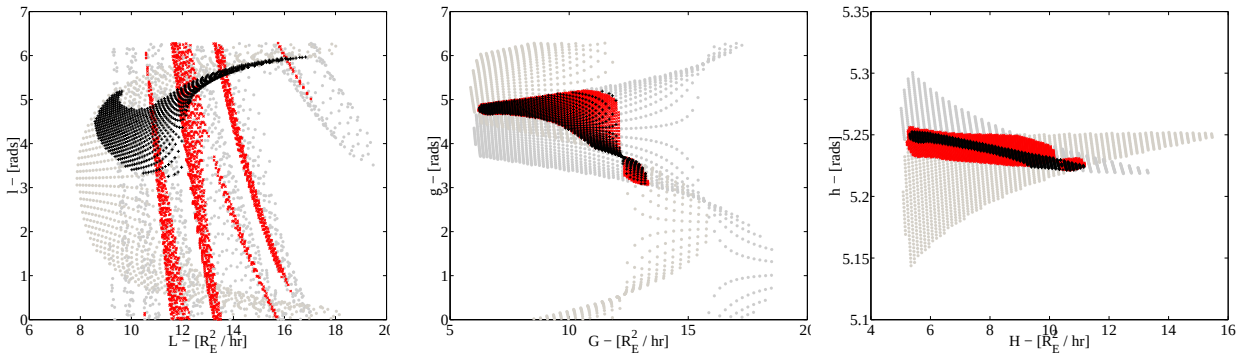

Figure 5: $T(70;0)\{\mathcal{A}^{rr}\}$ (red) and $T(70;70)\{\mathcal{A}^{rr}_{70}\}$ (black) projected onto the Delaunay planes, nonzenith observations

space. It is possible that further reductions can be made by continuing this process: cut away the nonoverlap region of the (G, g) plane, then do the same for the new nonoverlap region of the (H, h) plane, and continue to ping-pong back and forth until the intersection is known to within the desired uncertainty. Alternatively, since the actual orbit is now known to within a small neighborhood of a single point, a least squares solution can be carried out.

4 A Conceptual Algorithm

The purpose of this paper has been to introduce and illustrate the viability of this orbit determination technique. As such, all surface intersection reductions were carried out by hand. Future research must be done on the development of technology that efficiently automates this process. As intersections of two-dimensional surfaces must be performed, and not higher-dimensional surfaces, it is feasible to develop computationally efficient approaches for this. In this section we discuss an algorithm and indicate how one might use this technology in the orbit determination process and the subsequent inclusion of these new orbits in the space debris catalog when faced with a large number of observations per night. As was mentioned in §2.1, each observation should be recorded as an observation vector,

$$x = (A, t, L) \in \mathbb{R}^5 \times \mathbb{N},$$

that contains an attributable vector, the observation time, and the observatory's location. Each new observation should be checked against the catalog of known objects. If the observed attributable vector does not match any of the orbital particles in the catalog, it will be saved as an uncorrelated observation. A rolling observation window

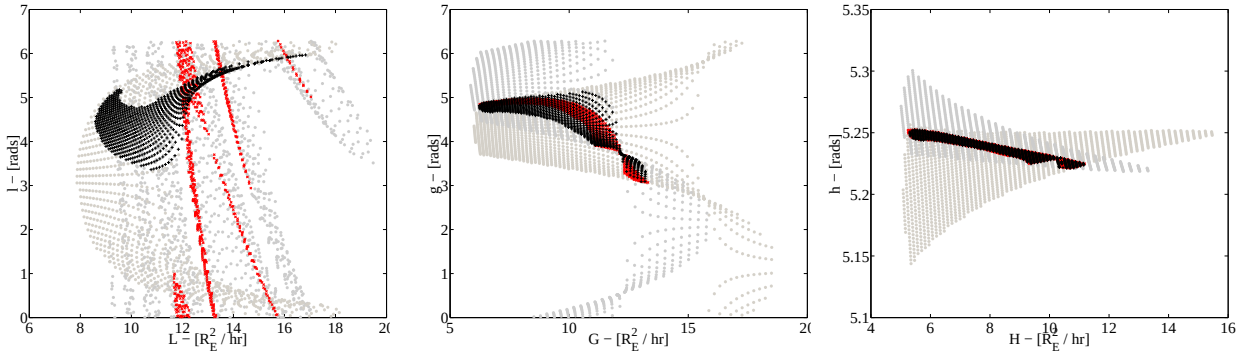

Figure 6: $T(70;0)\{\mathcal{A}^{rrr}\}$ (red) and $T(70;70)\{\mathcal{A}^{rrr}_{70}\}$ (black) projected onto the Delaunay planes, nonzenith observations

can be defined (for instance, one week) within which it is compared to all other uncorrelated observations. For these comparisons, a standard epoch time can be defined and all uncorrelated observations made within the observation window can then be mapped into the Delaunay planes and then dynamically evolved or regressed to the epoch time. These uncertainty projections can then be stored and intersected with all other such observations to discover which observations are correlated. For each orbit correlation that is found, the corresponding observations can then be saved in a secondary catalog, which is a temporary holding catalog, until the orbit is confirmed, at which time the data can be promoted to the primary catalog of correlated data.

The most difficult part of the routine is finding the common intersection point between the 2-D surfaces, or in finding what their minimum separation is. While the above, graphical based technique can in principle find these results, it is likely that a more analytical approach will ultimately be used. Such topics are currently being explored by our group.

5 Conclusion

This work is a preliminary study in which we propose a new conceptual procedure for carrying out orbit determination of space debris from two previously uncorrelated tracks observed with optical telescopes. We show how an optical track can be reduced to a four dimensional estimate of the sub-state and how the mapping of the admissible region into Delaunay space can be used to construct a notional algorithm for computing an orbit correlation and determination between two uncorrelated tracks. Our approach reduces the orbit correlation and determination process to performing intersections of two-dimensional laminas in the plane, a process we call Intersection Theory Analysis. For an example attributable vector we carry out this process as a proof-of-concept computation.

References

[1] Rossi, A., "Population Models of Space Debris." In: Milani, A., Knezevic, Z. (eds) it Dynamics of Population of Planetary Systems, Proceedings of IAU Coll., Vol. 197, CUP, 2005, pp. 427-438.

[2] Rossi, A., "The Earth Orbiting Space Debris," *Serb. Astron. J.*, Vol. 170, 2005, pp. 1-12.

[3] Tommei, G., Milani, A., and Rossi, A., "Orbit Determination of Space Debris: Admissible Regions," *Celestial Mechanics and Dynamical Astronomy*, Vol. 97, 2007, pp. 289-304.

[4] Maruskin, J.M., Scheeres, D.J., and Alfriend, K.T., "Correlation of optical observations of objects in Earth orbit," *Journal of Guidance, Control and Dynamics*, 2008, in press.

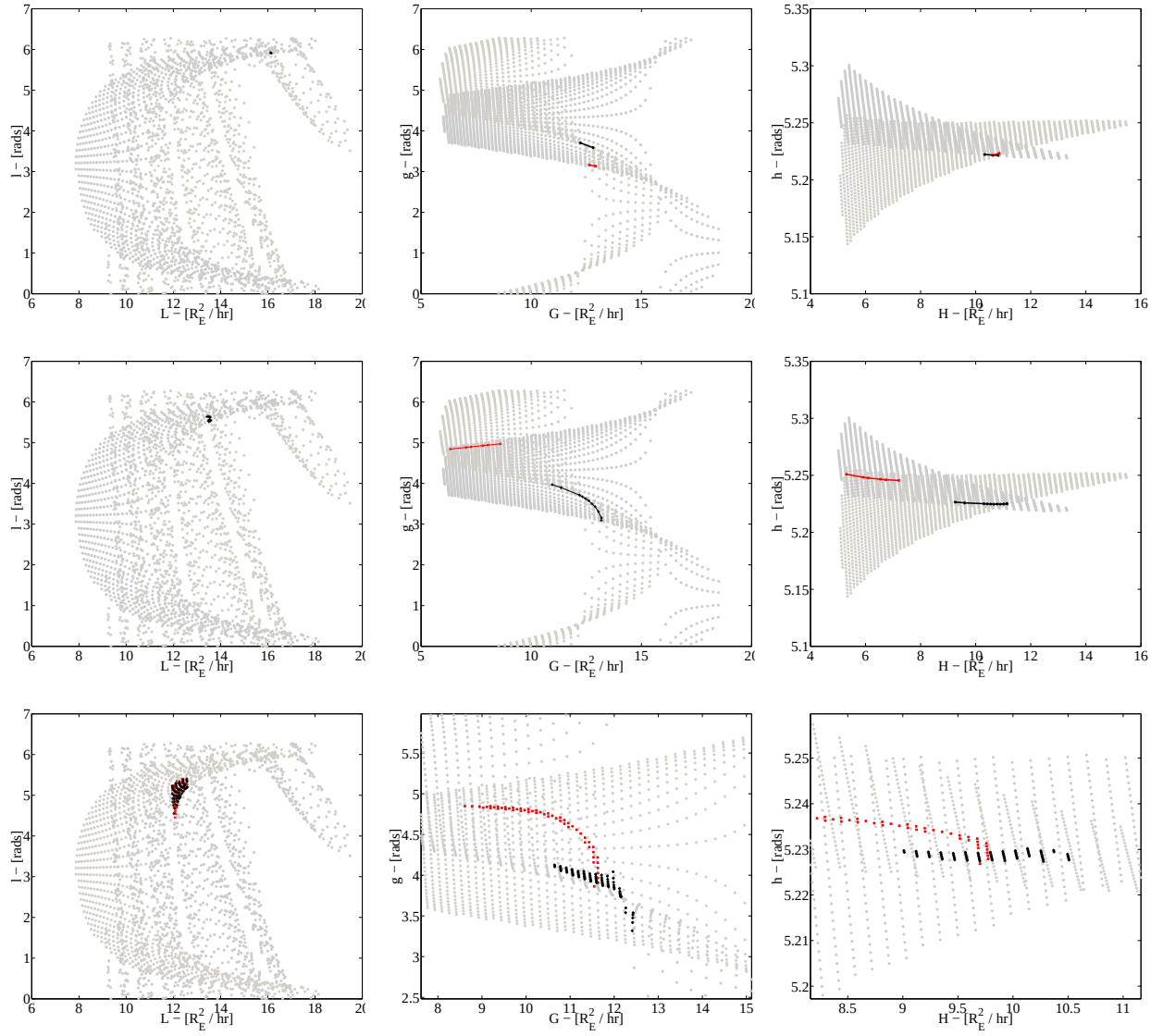

Figure 7: $T(70;0)\{\mathcal{A}^{rrrr}\}$ (red) and $T(70;70)\{\mathcal{A}^{rrrr}_{70}\}$ (black) projected onto the Delaunay planes, nonzenith observations

[5] Seitzer, P., Smith, R., Africano, J., Jorgensen, K., Stansbery, E., and Monet, D., "MODEST Observations of Space Debris at Geosynchronous Orbit," *Advances in Space Research* Vol. 34, No. 5, 2004, pp. 1139-1142.

[6] Milani, A., Knežević, Z., "From Astronomy to Celestial Mechanics: Orbit Determination with Very Short Arcs," *Cel. Mech. Dyn. Ast.*, Vol. 92, No. 1, 2005, pp. 1-18.

[7] Hamilton, T.W., and Melbourne, W.G., "Information Content of a Single Pass of Doppler Data from a Distant Spacecraft," *JPL Space Programs Summary*, Vol. 3, 1966, pp. 18 - 23.

[8] Ferraz-Mello, S., *Canonical Perturbation Theories: Degenerate Systems and Resonance*, Springer, 2007, pp. 1.